Kadlecova et al., https://doi.org/10.1083/jcb.201608071

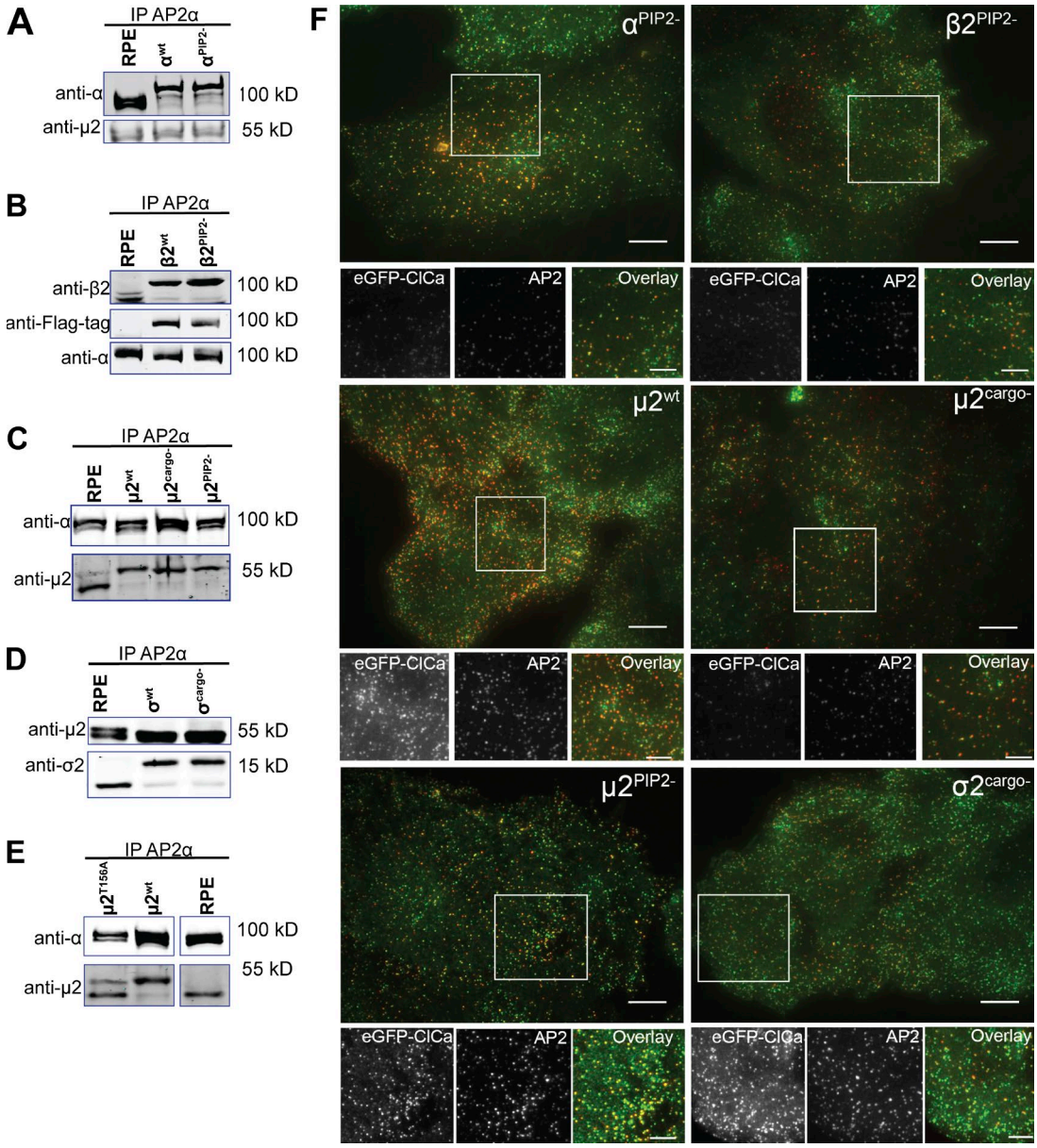

Figure S1. **Validation of AP2 mutant cell lines.** To ensure full incorporation of mutant subunits into intact AP2 complexes, antibodies against AP2 α were used to immunoprecipitate (IP) AP2 complexes from parental hTertRPE (RPE) or the indicated mutant cells expressing siRNA-resistant wild-type or mutant AP2 subunits after siRNA-mediated depletion of the endogenous subunit. Western blot analysis was performed against exogenously expressed WT or mutant subunit and a second endogenously expressed subunit using antibodies described in Materials and methods. (A) Cells expressing α^{wt} and α^{PIP2-} bearing a brain-specific insert in the flexible linker. (B) Cells expressing $\beta2^{wt}$ and $\beta2^{PIP2-}$ bearing a Flag epitope in the flexible linker. (C) Cells expressing $\mu2^{wt}$, $\mu2^{cargo-}$, and $\mu2^{PIP2-}$ bearing myc epitopes in the flexible linker. (D) Cells expressing $\sigma2^{wt}$ and $\sigma2^{cargo-}$ expressing Flag tags at their C terminus. (E) Cells expressing $\mu2^{T156A}$ bearing a myc tag in the flexible linker. Note in the latter case that the $\mu2^{T156A}$ mutant is inefficiently incorporated into AP2 complexes compared with endogenously expressed μ2. (F) Immunofluorescence localization of AP2 complexes containing mutated subunits α^{PIP2-}, $\beta2^{PIP2-}$, $\mu2^{cargo-}$, $\mu2^{PIP2-}$, and $\sigma2^{cargo-}$. Mouse monoclonal antibody against the AP2 α subunit was used to verify punctate pattern of AP2 complexes with mutated subunits at the plasma membrane and at the CCPs. Bars, 10 μm.

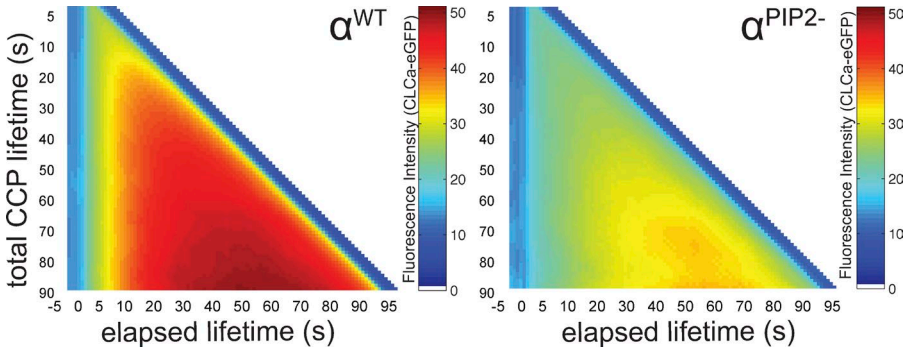

Figure S2. **Fluorescence analyses of clathrin intensity at CCPs in α^{PIP2-} cells show that efficient clathrin recruitment in the first 10–20 s predetermines stabilized and productive growth of a CCP.** The progression of CLC-EGFP recruitment at individual CCPs in α^{wt} (left) and α^{PIP2-} (right) cells is represented as a heatmap. Increase of CLC-EGFP intensity is plotted as a function of elapsed lifetime of a given CCP (*x*-axis), for all CCP lifetimes ranging from τ = 5 to 90 s (*y*-axis). Total CCP lifetime is on the *y*-axis (top, short lifetimes; bottom, long lifetimes), the current "age" of the CCP is on the *x*-axis from left to right (the data stops at the diagonal because CCP age can never be greater than total lifetime). CLC-EGFP intensity is depicted as the color at each location. The fluorescence intensity profiles in α^{wt} cells show clearly defined transitions (blue to green to yellow to red) at early stages of CCP lifetime at the left side of the α^{wt} heatmap, indicative of highly regulated CCP growth and maturation. This also suggests that CCPs that recruit clathrin at a net faster rate in the first 10–20 s are the ones that will have long lifetimes and ultimately grow to larger sizes, as apparent from the total overall amount of CLC-EGFP. In contrast, transitions are blurred in the α^{PIP2-} cells, and the relative maximum intensity at each lifetime is reached much later (i.e., at longer CCP ages). The CCP intensities in the α^{PIP2-} cells are significantly lower than in α^{wt} cells, indicating defects in growth and maturation.

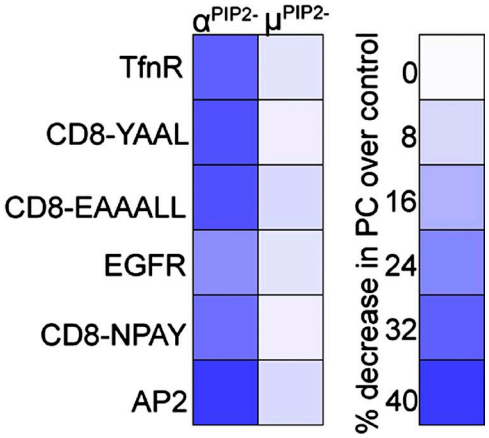

Figure S3. **Abrogation of α–PIP2 interactions leads to a general cargo sorting defect.** Heatmap representing the relative changes in Pearson correlation coefficient (PC) between EGFP-CLCa and the indicated CD8 chimeras and other CME cargo showing more severe defects in cargo loading into CCPs in α^{PIP2-} cells compared with $\mu2^{PIP2-}$ cells. AP2 recruitment and stabilization at CCPs is also reduced in the α^{PIP2-} cells, but not in $\mu2^{PIP2-}$ cells.

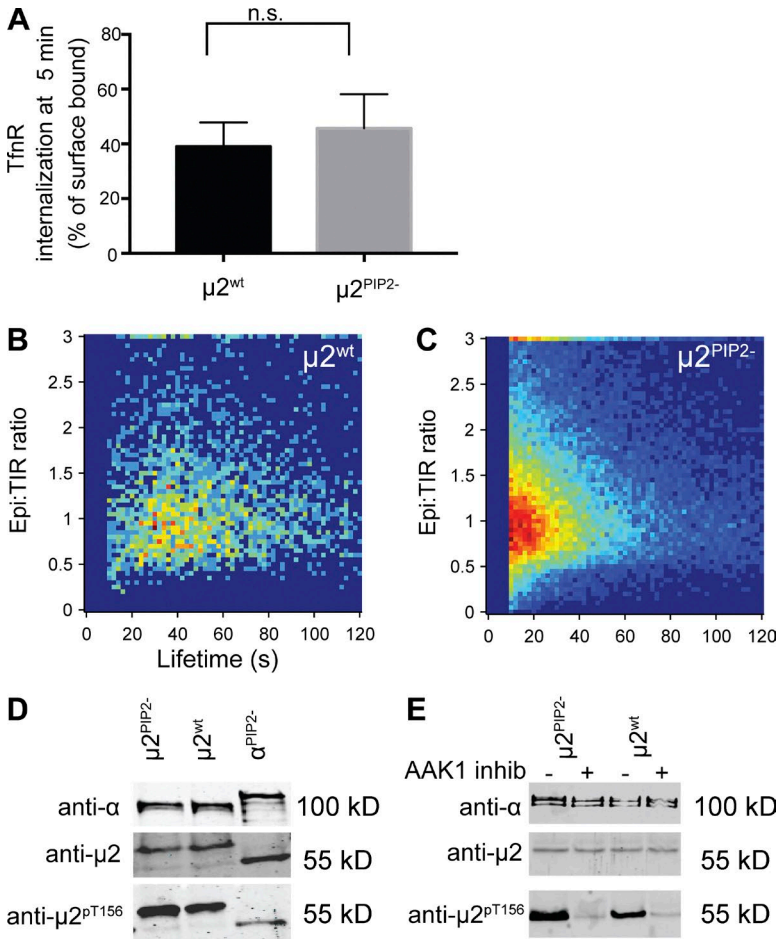

Figure S4. **$\mu2^{PIP2-}$ cells show no apparent defect in TfnR endocytosis but have a defect in CCP maturation, and efficient CME is restored by activation of AAK1 kinase and increased phosphorylation of μ2.** (A) Transferrin receptor internalization was measured in control and $\mu2^{PIP2-}$ cells using a monoclonal anti-TfnR antibody as ligand. TfnR uptake after 5 min, which is reflective of the rate of TfnR uptake, was calculated as a percentage of the initial total surface-bound antibody. Data represent mean ± SD, $n = 3$. n.s., not significant. (B and C) Epifluorescence (Epi)/TIR ratio, which is indicative of curvature acquisition, for individual CCPs plotted as a function of CCP lifetime in μ2WT (B) and $\mu2^{PIP2-}$ cells (C), as indicated. $\mu2^{PIP2-}$ cells exhibit 2.5-times increased numbers of short-lived, flat, and presumably abortive CCPs, indicative of a defect in CCP maturation. (D) AP2 complexes were immunoprecipitated with anti-α mAb and then subjected to Western blotting using anti-μ2 and anti-T156 phospho-μ2 antibodies as indicated. $\mu2^{PIP2-}$ cells exhibit an increase μ2 phosphorylation on residue T156 relative to $\mu2^{wt}$ cells, whereas μ2 phosphorylation is decreased in α^{PIP2-} cells. (E) Treatment with the AAK1 inhibitor, Compound 2, decreases μ2pT156 levels in both μ2wt and $\mu2^{PIP2-}$ cells.

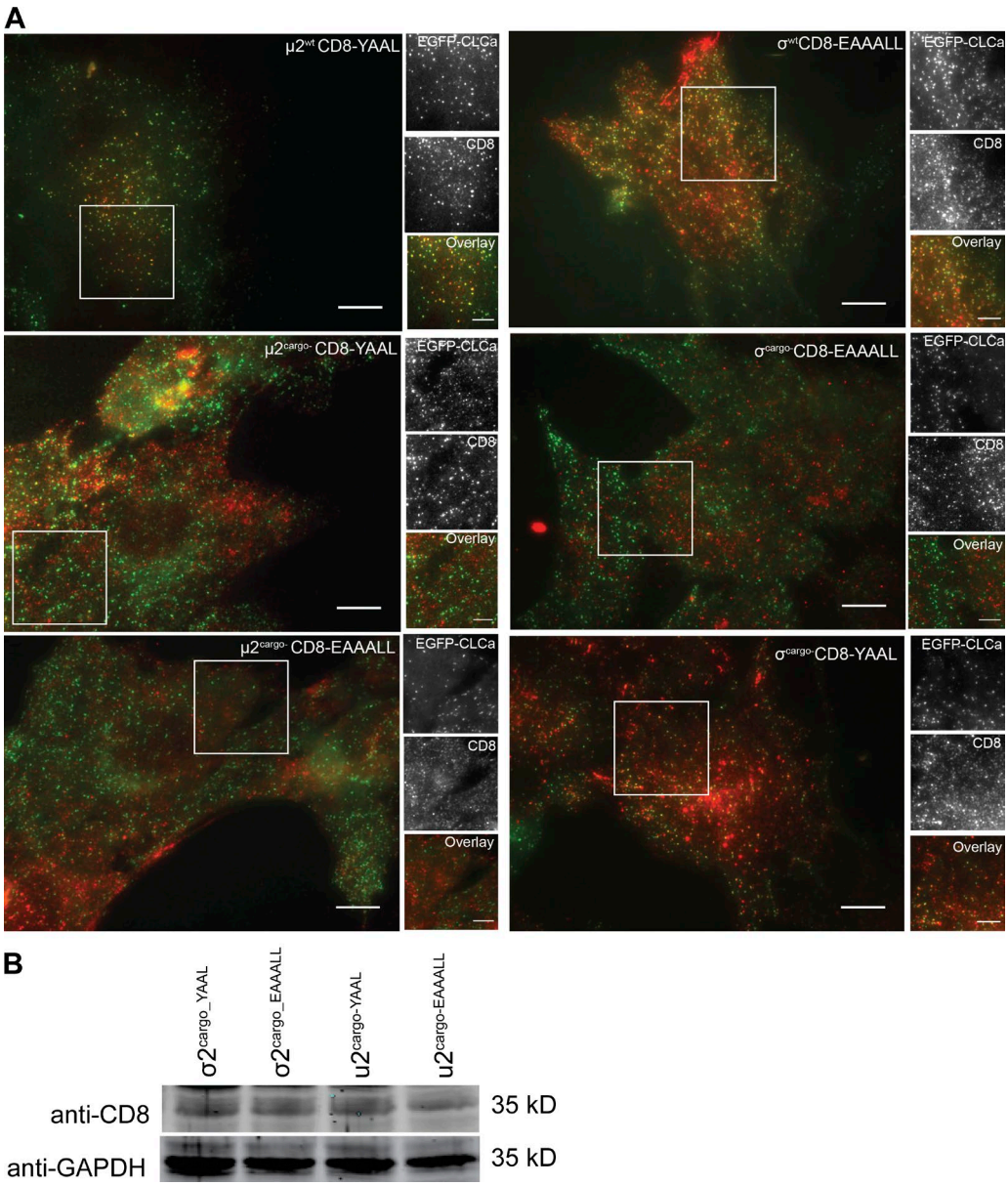

Figure S5. **Adenoviral-mediated expression of model cargo receptors in htertRPE cells.** (A) Immunofluorescence showing colocalization of model cargo CD8-YAAL or CD8-EAAALL detected with mouse monoclonal antibody UCHT-4 against CD8 relative to EGFP-CLCa in WT, $\mu2^{cargo-}$, or $\sigma2^{cargo-}$ mutant cells as indicated. Bars, 10 µm. (B) Western blot showing equal levels of expression of CD8 chimeras in $\mu2^{cargo-}$ and $\sigma2^{cargo-}$ cells.

Provided online is a zip file that includes the custom Python and R scripts used for all computational analyses conducted in this study.